Low Temperature Physics/Fizika Nizkikh Temperatur, 2015, v. 41, No. 6, pp. 564–570

Melting of cryocrystals at high pressures. Computer simulation

E.S. Yakub

Cybernetics Dept., Odessa National Economic University, 8 Preobrazhenskaya, Odessa 65082, Ukraine
E-mail: yakub@oneu.edu.ua

Received October 8, 2014, published online April 23, 2015

Simple molecular models were applied to predict melting temperature of highly compressed classical molecular crystals of hydrogen and nitrogen in a wide range of pressures and temperatures using conventional molecular dynamics simulation. It was shown that models which comprise noncentral interaction can reproduce turnover of the melting line observed at megabar pressures. We discuss the relation of this effect to the parameters of chemical bonding.

PACS: 67.80.F– Solids of hydrogen and isotopes;
67.63.Cd Molecular hydrogen and isotopes;
64.60.Ej Studies/theory of phase transitions of specific substances;
31.15.xv Molecular dynamics and other numerical methods.

Keywords: molecular dynamics, high-pressure melting, hydrogen, nitrogen.

1. Introduction

Maximum of melting temperature predicted in *ab initio* simulations [1] of highly compressed molecular hydrogen has been extensively discussed in the literature during the last years. Despite serious difficulties in measurements at megabar pressures and elevated temperatures, experimentalists worked hard to verify the existence of such a maximum. Several research groups have confirmed the turnover in the melting line of hydrogen [2–4]. A similar behavior of the melting line was observed in nitrogen at pressures 50–80 GPa [5,6].

There are different points of view on what the physics is behind this effect, in particular, specific changes in the intermolecular interaction during melting have been assumed as its reason [1]. However, discovery of similar maxima of melting temperature in other simple molecular systems, particularly in carbon and water [5], gave some grounds to consider that the origin of the turnover effect may have a more general reason.

The aim of this work is an attempt to find such a general reason for the turnover of the melting line in simple diatomic solids. Our way of studying melting of highly compressed classical diatomic crystals is straightforward. We applied classical molecular dynamics (MD) simulation combined with simplest molecular models including isotropic (spherically averaged) potential model, atom–atom potential (AAP) and diatom–diatom potential approximation (DDP) [7]. Two types of such simulations: conventional single-box and two-phase MD were used and compared with *ab initio* predictions [1] and existing experimental data [2–6].

In the next section we describe molecular interaction models for molecular hydrogen and nitrogen. Section 3 provides details of MD simulations performed. The comparison of results with experimental and *ab initio* simulation data and general discussion are presented in Sec. 4, conclusions are formulated in the last section.

2. Potential models for H_2–H_2 interaction

Interaction of hydrogen molecules was the subject of many studies (see e.g., monograph [8] and recent paper of Freiman *et al.* [10]). Most of them have been based on semi-empirical isotropic potentials, which consider the anisotropy of intermolecular interaction as a small correction and ignore interplay between inter- and intramolecular coordinates. This approach is quite reasonable at low temperatures and densities where rotational and vibrational excitations play a minor role.

Isotropic potential model

The simplest molecular potential model we considered takes into account only isotropic part of intermolecular interaction. Within such isotropic potential model the interaction energy of N_m molecules is represented by an additive sum of all $N_m(N_m - 1)/2$ central pair potentials $V_{\text{is}}(r_{ij})$. Several isotropic potentials proposed for hydrogen

molecules are discussed and compared in Ref. 8. All of them (except the Lennard-Jones potential at very short distances) are close to the potential proposed by Silvera and Goldman [9]. In this work we use a simple three-parametric Morse function:

$$V(r) = \varepsilon\left[e^{-2\beta(r-r_0)} - 2e^{-\beta(r-r_0)}\right], \qquad (1)$$

with: ε/k_B = 33 K, r_0 = 3.424 Å, β = 1.701 Å, as an approximation for this potential.

AAP model

Another relatively simple model (see e.g., Ref. 8) applied in this work is AAP approximation [7]. According to AAP model, potential energy of N homonuclear diatomics can be represented as a function of interatomic distances of all their $2N$ constituent atoms:

$$U_{2N} = \sum_{(ij)} U(L_{ij}) + \sum_{i<j} \Phi(r_{ij}). \qquad (2)$$

Here $U(L_{ij})$ is intramolecular potential energy of a diatomic molecule and nonbonding atom–atom potential $\Phi(r_{ij})$ describes interactions between atoms bound in different molecules. $U(L_{ij})$ is a function of the distance between ith and jth atoms forming this molecule (i.e., of the instant bond length L_{ij}). Correspondingly, the first sum in Eq. (2) extends over all N_m molecules, and the second is taken over all $4\,N_m(N_m - 1)$ pairs of atoms belonging to different molecules.

It was used in a wide range of applications, where short-range noncentral interactions of diatomic molecules, their nonrigidity, rotational and vibrational excitations become important: from evaluating the third virial coefficient of dissociating hydrogen and calculating structure, thermodynamic and transport properties, up to predicting polymorph transitions in solid H_2 and Hugoniots of fluid hydrogen [7,11–14].

First theoretical justification of AAP model, based on expansion of London's potential surfaces of four hydrogen atoms under valence bond theory [19], was later reformulated in a more general form suitable for arbitrary systems of diatomic molecules in their singlet ground states within the framework of molecular orbital method (Böhm–Ahlrichs theorem [16]). According to this theorem, the nonbonding atom–atom potential $\Phi(r_{ij})$ can be expressed as a weighted average of interaction energies of two isolated atoms over all their electronic terms. In the particular case of molecular hydrogen the intramolecular potential corresponds to the ground (singlet) state of H_2 molecule: $U(r) = u(^1\Sigma\,|\,r)$ and intermolecular atom-atom potential $\Phi(r)$ is the sum of 1/4 of singlet $u(^1\Sigma\,|\,r)$ and 3/4 of triplet $u(^3\Sigma\,|\,r)$ potentials of H_2 molecule:

$$\Phi(r) = \frac{1}{4}u(^1\Sigma\,|\,r) + \frac{3}{4}u(^3\Sigma\,|\,r). \qquad (3)$$

Both singlet and triplet potential curves are well known from the classical *ab initio* variational calculations of Kolos and Wolniewitz [17]. Aiming to investigate the location and shape of the melting curve $T_m(P)$ of the classical highly compressed molecular hydrogen we applied in this work the AAP model in the same form as in our previous studies [7,11–14]. Potential energy of the singlet ground state of H_2 $u(^1\Sigma\,|\,r)$ was represented by the modified Hulburt–Hirschfelder potential:

$$U(r) = D_e\left[e^{-2x} - 2e^{-x} - ax^3(1-bx)e^{-cx}\right], \qquad (4)$$

where $x = \beta(r/r_e - 1)$, r_e = 0.74126 Å, D_e = 4.747 eV, β = 1.4403, a = 0.1156, b = 1.0215, c = 1.72 [16]. Equation (4) provides an excellent approximation for $^1\Sigma_g^+$-curve [17] within a wide range of distances (0.3–5 Å). Approximation for nonbonding atom–atom potential $\Phi(r)$ was proposed by Saumon and Chabrier [20]:

$$\Phi(r) = \varepsilon\left[\gamma e^{-2s_1(r-r^*)} - (1+\gamma)e^{-s_2(r-r^*)}\right]. \qquad (5)$$

Equation (5) gives an accurate description of nonbonding interaction of hydrogen atoms Eq. (4) in a wide interval of distances (0.5–6.5 Å), including regions of strong repulsion at short distances and weak dispersion attraction at larger distances. We used parameters of the potential Eq. (5) determined in Ref. 20 on the basis of *ab initio* calculations of Kolos and Wolniewitz [17]: r^* = = 3.2909 Å, $\varepsilon = 1.74\cdot10^{-3}$ eV, γ = 0.4615, s_1 = 1.6367 Å^{-1}, and s_2 = 1.2041 Å^{-1}.

DDP model

Another potential model used in this work was DDP approximation [7]. It is actually a more general version of AAP model which takes into account the overlap of electronic shells of two atoms forming a diatomic molecule. Within this approximation nonbonding short-range intermolecular interaction depends on instant distances between bonded atoms.

According to DDP model, nonbonding interaction of ith atom (forming a diatomic molecule with atom k), with jth atom (bonded in another diatomics to atom l), can be expressed as follows:

$$\Phi_{DDP}(r_{ij}) = \frac{1}{2}\left[g(L_{ik}) + g(L_{jl})\right]\Phi(r_{ij}). \qquad (6)$$

Functions $g(L)$, depending on instant chemical bonds lengths, can be expressed via corresponding overlap integrals $S(L)$: $g(L) = [1 + S^2(L)]^{-2}$. Below we use the well-known expressions [20] for these overlap integrals

$$S = \left(1 + w + \frac{w^2}{3}\right)\exp(-w), \quad w = \left(1 + \frac{4.075}{2.643 + (r/a_0)^2}\right)\frac{r}{a_0},$$

where a_0 is Bohr radius.

AAP+QQ and DDP+QQ models

Both AAP and DDP approximations ignore the long-ranged electrostatic interaction which is important e.g., in description of orientational polymorph transitions in diatomic solids [7]. The leading kind of such interaction, namely quadrupole–quadrupole (QQ) interaction, when added to AAP and DDP models, gives new potential models, referred below, correspondingly, as AAP+QQ and DDP+QQ models.

This quadrupole–quadrupole contribution can been written as [8]:

$$\Phi_{QQ}(R,L_1,L_2)=\frac{3}{4}\frac{Q(L_1)Q(L_2)}{R^5}\times$$

$$\times\Big[1-5\,(\boldsymbol{\omega}_1\cdot\mathbf{n})^2-5\,(\boldsymbol{\omega}_2\cdot\mathbf{n})^2+2(\boldsymbol{\omega}_1\cdot\boldsymbol{\omega}_2)^2+$$

$$+35(\boldsymbol{\omega}_1\cdot\mathbf{n})^2(\boldsymbol{\omega}_2\cdot\mathbf{n})^2-20(\boldsymbol{\omega}_1\cdot\mathbf{n})(\boldsymbol{\omega}_2\cdot\mathbf{n})(\boldsymbol{\omega}_1\cdot\boldsymbol{\omega}_2)\Big], \qquad (7)$$

where $Q(L)$ are quadrupole moments of interacting molecules, depending on their instant bond lengths, $\boldsymbol{\omega}_1$, $\boldsymbol{\omega}_2$ and $\mathbf{n}$ are unit vectors defining, correspondingly, directions of molecular axes, and "center-to-center" vector $\mathbf{R}$, $R=|\mathbf{R}|$ is the distance between molecular centers. Quadrupolar forces acting between hydrogen molecules are studied very well [8] and molecular quadrupole moment as a function of the bond length is known from *ab initio* calculations of Kolos and Wolniewitz [18]. We used the following its approximation:

$$Q_{H_2}(L)=Q_{H_2}(r_e)\Big[1+1.733\Delta r+0.932\Delta r^2\Big]. \qquad (8)$$

Here $Q_{H_2}(r_e)=-0.486$ a.u. is quadrupole moment at equilibrium distance r_e = 0.74126 Å, and $\Delta r=L-r_e$ is the instant deviation of the bond length from this equilibrium distance (in Å).

It should be stressed that all above potential models proposed for description of molecular interaction in compressed hydrogen are nonempirical, i.e., they all have no parameters fitted using experimental data. Therefore before applying these models in predicting the melting line of molecular hydrogen it is reasonable to estimate their quality by comparing their predictions with available high-pressure measurements.

In Fig. 1 we compare pressure, computed in MD simulation (see the next Section for details) with measurements of Akahama *et al.* [21] at T = 100 K. As one can see, the pressure predicted using the isotropic potential model is extremely overestimated. AAP+QQ model is better but is still unsatisfactory at pressures higher than 50 GPa. Pressures predicted by DDP+QQ model are in a better agreement with the experiment. At megabar pressures this model underestimates pressure by 10–15%.

At the same time this comparison is not completely correct because at T = 100 K solid hydrogen is still essentially quantum crystal whereas our MD simulation is purely classical. To estimate possible influence of quantum effects we invoke below the well-known Feynman's variational approach [13].

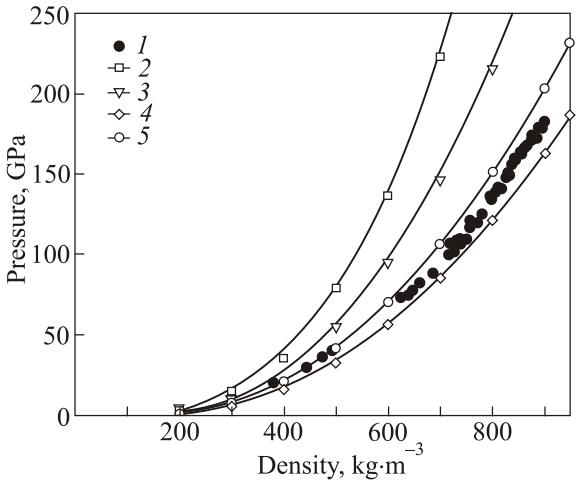

Fig. 1. Comparison of MD simulation results (512 atoms) for different models of solid H_2 with measurements of Akahama *et al.* [21] at T = 100 K: *1* is experimental data [21]; *2* is isotropic potential model Eq. (1); *3* is AAP+QQ model Eqs. (2), (4), (5); *4* is DDP+QQ model Eqs. (2), (4), (6); *5* is DDP+QQ model with quantum corrections Eq. (8)

According to this approach, one can approximately calculate the free energy of a quantum system using classical methods if its potential energy $V(r)$ is replaced by an effective potential defined as

$$\tilde{V}(r,T)=\frac{1}{\sqrt{\pi}}\int_{-\infty}^{+\infty}V\left(r+\lambda t\right)\exp(-t^2)\,dt, \qquad (9)$$

where $\lambda=\hbar/\sqrt{6mkT}$ and m is mass of interacting particles. For example, to estimate possible quantum effects in the case of the exponential repulsion $V(r)=A\exp(-br)$ one can simply replace the pre-exponential factor A by $A\exp(\lambda^2b^2/4)$. Curve *5* in Fig. 1 was calculated using DDP+QQ model with such replacements in all pre-exponential factors of Eq. (5). As one can see, the estimated quantum corrections are of the same order of magnitude as the deviations of pressures from experimental data predicted by classical DDP model from experimental data.

Potential model for N_2–N_2 *interaction*

In simulation of melting of nitrogen solid we applied a semi-empirical version of AAP model, used earlier in prediction of thermodynamic properties of nitrogen fluid at high temperatures and pressures [22].

Intramolecular potential $U(r)$ for N_2 molecules was described by the same Morse potential Eq. (1) with parameters $\varepsilon=9.91$ eV, $r_0=1.0975$ Å $\beta=2.963$ Å^{-1}. Nonbonding potential of intermolecular atom–atom interaction $\Phi(r)$, estimated in [22] on the basis of Böhm–Ahlrichs

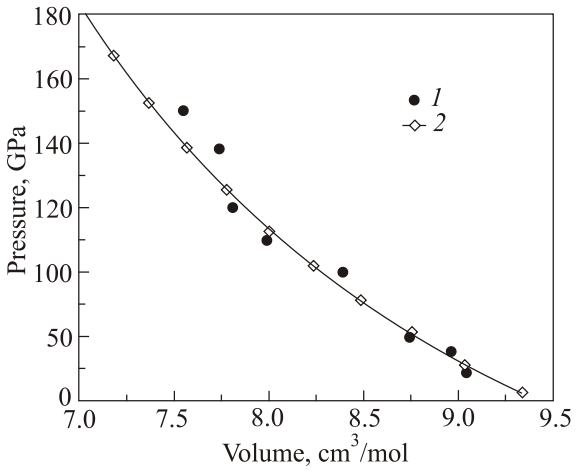

Fig. 2. Comparison of MD simulation results (512 atoms in the box) with experimental data for solid nitrogen at room temperature: *1* is measurements of Eremets *et al.* [23]; *2* is simulation data based on semiempirical AAP model.

theorem, was replaced by empirical Morse function Eq. (1). Its parameters $\varepsilon/k_B = 50$ K, $r_0 = 3.62$ Å, $\beta = 1.65$ Å^{-1} were found by fitting the measured high-density *P*–*V*-data of Eremets *et al.* [23] as shown in Fig. 2.

3. Molecular dynamics simulation

To locate the melting line of the classical molecular H_2 and N_2 solids, we carried out a series of conventional single-box Nose-Hoover *NV-T* MD simulations at temperature above 300 K. The main technical details of these simulations are presented in Table 1. To keep an eye on possible effect of the periodical boundary conditions (PBC) on the phase transition parameters we carried out simulations using two different sizes of MD-box: 512 atoms (256 molecules) and 1782 atoms (864 molecules).

Each simulation starts from an initial configuration generated at a given fixed density and room temperature in a cubic box with molecular centers forming a close-packed (fcc) crystalline structure and all intramolecular distances corresponding to the equilibrium bond length. After equilibration a long MD run was performed to test the stability of the crystalline structure as explained below. When the initial crystalline structure survived during this period, the initial state was attributed to the solid phase, the temperature increased by 25 K and simulation repeated until melting occurs. Then the same procedure was repeated at a new density etc.

Table1. Adopted parameters of MD simulation

Number of atoms in the box	512 … 1782
Cut-off radius of potential, Å	H_2: 4.7 N_2: 6.5
Time step, fs	0.125
Equilibration period, ps	10
Period of MD-run, ps	300
Periodicity of data storing, ps	2.5
Interval of densities, $g\cdot$cm^{-3}	H_2: 0.3–1.0 N_2: 1.5–4.5

Several types of initial orientations of molecules in crystalline lattice were tested but no effect on the final simulation results was found, because molecular rotations and vibrations at high temperature are so intense that details of the initial static orientations are quickly forgotten.

The instant values of all atomic coordinates, as well as pressure, energy, mean chemical bond length have been periodically stored in files for further analysis. Establishing and maintaining of thermodynamic equilibrium was monitored continuously on the screen by comparing the actual and Maxwellian velocity distributions. We controlled also the proper choice of the Nose–Hoover thermostat coupling parameter to avoid large fluctuations of temperature in MD box.

To detect melting at a given density, the radial distribution function and mean squared displacements of molecular centers in MD box were periodically examined. Additional test of the crystalline structure stability was done by visualizing instant positions of all atoms inside the box using JMol java viewer [24]. Eventually we were able to detect the maximum temperature corresponding to the crystalline state remaining stable during the whole MD simulation run.

4. Results and discussion

Results of our MD simulations are presented in Figs. 3–5. In Fig. 3 the melting temperatures of hydrogen predicted using five different potential models described in Sec. 2 are compared with experimental data of Deemyad and Silvera [2], Gregorianz *et al.* [26], and Eremets and Troyan [3] as well as with the results of *ab initio* simulations of Bonev *et al.* [1]. The most interesting here was the pronounced turnover of the melting line, found in all our simulations except for one based on the isotropic molecular model. The same effect was observed in the case of molecular nitrogen (Fig. 4).

It is worth to mention here that strictly speaking it is impossible to determine the exact location of the melting line using such single-box MD technique. In our simulation we were actually able to detect the limit of the lattice stability, which can be regarded as an upper bound of the melting temperature. This limit may exceed the real thermodynamic melting temperature T_m because the crystals may exist in metastable states at $T > T_m$. According to existing estimations the achievable overheating of van-der-Waals' crystals expected to be rather small [25].

To verify this assumption a few additional simulations were carried out using an alternative method of the initial state generation when one or two layers of crystalline lat-

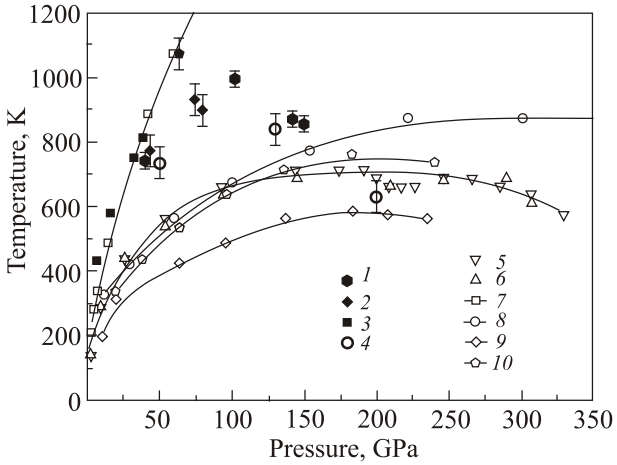

Fig. 3. Melting line of molecular hydrogen. Comparison of predicted melting temperatures (open symbols) with *ab initio* and experimental data (solid symbols). *1* is Eremets and Troyan [3]; *2* is Deemyad and Silvera [2]; *3* is Gregoryanz *et al.* [26]; *4* is Bonev *et. al* [1]; *5* is AAP model (512 atoms); *6* is AAP model (1728 atoms); *7* is isotropic potential (864 molecules); *8* is AAP+QQ model (512 atoms); *9* is DDP model (512 atoms); *10* is DDP+QQ model (512 atoms).

tice in the initial configuration were disordered. If the crystalline structure was recovered during simulation, this state was attributed to the solid, otherwise it was considered as a liquid phase. We refer below to such approach as to "two-phase simulation". It gives the possibility to estimate the lower bound of the melting temperature. Results of such simulations of the nitrogen solid shown in Fig. 4 confirm that the overheating at high pressures does not exceed a few percent of the estimated melting temperature. The

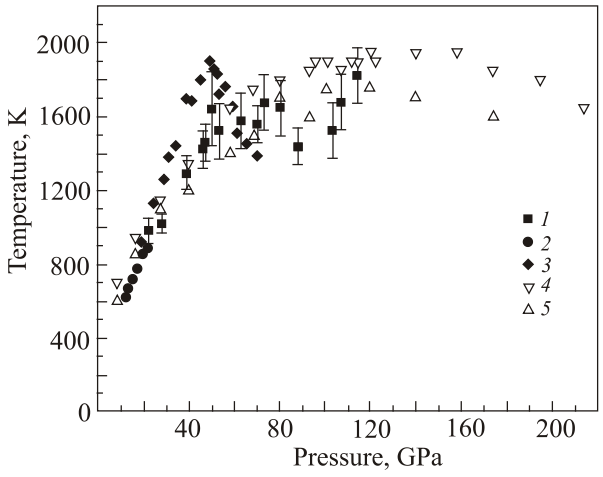

Fig. 4. Melting line of molecular nitrogen. Comparison of MD predictions data based on AAP+QQ model (open symbols) with experimental data (solid symbols). Experimental data: *1* is Goncharov *et al.* [6]; *2* is Zinn *et al.* [15]; *3* is Mucherjee and Bohler [5]; this work (1728 atoms): *4* is single-box; *5* is two-phase simulation.

agreement between predicted and measured melting temperatures here is satisfactory up to P = 100 GPa but the maximum of the melting temperature occurs at higher pressures, corresponding to stable polymeric phase [27] where experimental data are absent.

We found no significant effect of PBC on our simulations, except for the small boxes at the highest densities studied [31]. We attribute it to an artificial periodicity imposed by PBC.

In order to clarify the main question: what the physics is behind the overall turnover of the melting line, a few additional MD experiments on hydrogen were carried out by varying potential parameters responsible for chemical bonding in AAP model.

These results are presented in Fig. 5. The first simulation was intended to shed light on the role of the nonspherical part of intermolecular interaction. In the first series of simulations the equilibrium bond length — parameter r_e in Eq. (4) was shortened by half (curve *4*). Much more steep raise of the melting temperature in this case when compared to the predictions of standard AAP model (curve *3*) indicate the importance of nonspherical part of short-range molecular interaction in explanation of the melting line turnover effect.

Second and third experiments have been carried out to assess the role of the chemical bond rigidity. We re-estimated the location of the melting line using the same AAP model with different stiffness of the chemical bond. In the second experiment the parameter β in Eq. (3), responsible for vibronic frequency, was reduced by half (curve *2*) and in the third one it was doubled (curve *5*).

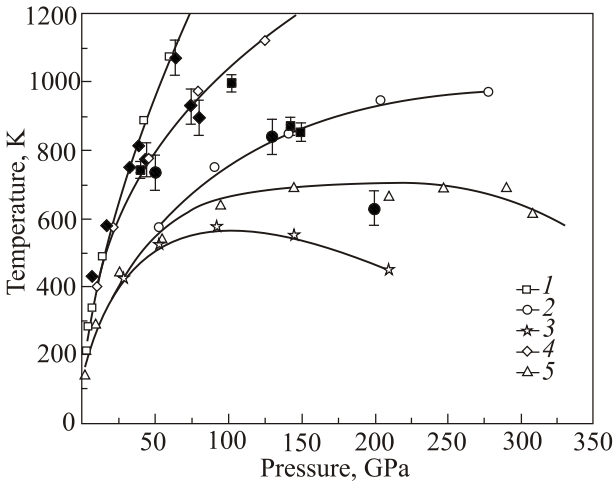

Fig. 5. Effect of chemical bonding factor on the melting temperature of hydrogen. Gray signs represent the same experimental and *ab initio* data as in Fig. 3. Solid lines represent melting curves predicted using: *1* is isotropic potential model Eq. (1); *2* is AAP model with stiffness parameter β reduced by half; *3* is standard AAP model with parameters according to Eq. (4); *4* is the same model with equilibrium bond length r_e shortened by half; *5* is the same model with doubled stiffness parameter β.

As one can see, the stiffness of the chemical bond at a fixed its equilibrium length also plays an important role in the shape of the melting curve. The stiffer is the chemical bond (and, correspondingly, the higher is the vibronic frequency), the more pronounced is the turnover of the melting line.

It is worth to mention also the specific shape of the melting line near the maximum of its melting temperature, the secondary effect found already in our preliminary AAP simulations [28], which can be clearly seen in Fig. 3. Just after first maximum of the melting temperature predicted at $P \sim$ ~ 170 GPa, there appears an apparent flattening (or even a notch) located just at pressure around 200 GPa. According to estimation of Silvera and Deemyad [29], the phase I – phase III polymorph transition line crosses the predicted melting line just in this region. Taking into account the fact that AAP model reproduces the orientational ordering of hydrogen molecules in solid phase [13], one may speculate that the right part of the melting line at $P > 200$ GPa corresponds to the melting of a more orientationally ordered phase of the solid hydrogen.

Although we did not determine in our simulations the density of coexisting phases and did not assess the volume jump at melting, some conclusions about it can be made indirectly analyzing obtained MD data. It was found that in the whole range of pressures studied, the melting process at a fixed density in MD box, except highest densities, is accompanied by a certain increase of the internal energy $\Delta u = u_{\rm liq} - u_{\rm sol}$. Small changes in pressure observed at melting are different at low and high densities. Pressure in MD box slightly decreases during the melting at lower densities, where the slope of $T_m(P)$ is positive, and increases at higher densities where function $T_m(P)$ decreases. Such behavior is consistent with the standard thermodynamic constraints that require lower density of the liquid phase in the region of the positive slope of $T_m(P)$ and *vice versa*. Volume jumps estimated using the Clausius–Clapeyron relation and obtained values of Δu, dT_m/dP, are very small, ranging from +0.05 cm^3/mol at low pressures up to –0.03 cm^3/mol at pressures $P > 300$ GPa.

5. Conclusions

Summarizing the above discussion, one may conclude that turnover in the melting line of simple diatomic solids like hydrogen or nitrogen can be explained in general on the basis of simple molecular models. We believe that the decrease of the melting temperature at high compressions is related to the increasing role of noncentral forces and molecular rigidity. The short-range atom–atom repulsion hinders molecular rotation and leads eventually to the progressive shortening of the chemical bonds and to the increase of vibronic frequency and intramolecular energy in the solid phase under increasing pressure.

The reason for the turnover effect, in our opinion, is a kind of frustration experienced by nonspherical molecules placed in sites of a crystal lattice. This frustration, related to deformation of the chemical bonds progressing with an increasing density in orientationally ordered phase of solid hydrogen is partially released at melting. According to our simulations, the mean bond length in H_2 molecules continuously decreases with an increasing pressure both in solid and liquid phases (from 0.74 Å at low pressures up to 0.69 Å at 300 GPa) but in the liquid it always remains longer. The same reason, in our opinion, caused flattening of the melting curve of hydrogen predicted in NVE simulations of Davis *et al*. [30].

Note that this effect is manifested for a number of interaction models, common for solid and liquid phases. This fact contradicts the assumption of Bonev *et al.* [1] that for turnover of the melting line are responsible some changes in intermolecular interaction which occur during melting.

It should be also noted that inclusion of quadrupole-quadrupole interactions leads to a noticeable increase of the predicted melting temperature, especially at relatively low densities, but does not change its overall behavior. Quadrupole forces affect mainly the nature of the molecular rotation in the solid phase and the type of the most stable crystalline structure. At pressures below 100 GPa one needs to take into account quantum effects for better reproducing the observed location of the melting line of molecular hydrogen. At pressures higher 250 GPa an additional consideration of the ionization effects [31,32] on the shape of the phase diagram is required.

1. S.A. Bonev, E. Schwegler, T. Ogitsu, and G. Galli, *Nature* **431**, 669 (2004).
2. S. Deemyad and I.F. Silvera, *Phys. Rev. Lett*. **100**, 155701 (2008).
3. M.I. Eremets and I.A. Trojan, *JETP Lett*. **89**, 198 (2009).
4. N. Subramanian, A.F. Goncharov, V.V. Struzhkin, M. Somayazulu, and R.J. Hemley, *Proc. Natl. Acad. Sci. USA* **108**, 6014 (2012).
5. G.D. Mucherjee and R. Bohler, *Phys. Rev. Lett*. **99**, 225701 (2007).
6. A.F. Goncharov, J.C. Crowhurst, V.V. Struzhkin, and R.J. Hemley, *Phys. Rev. Lett*. **101**, 095502 (2008).
7. E.S. Yakub, *Physica B: Cond. Mat*. **265**, 31 (1999); *J. Mol. Liq*. **93**, 69(2001).
8. *Physics of Cryocrystals*, V.G. Manzhelii and Yu.A. Freiman (eds.), AIP (1997).
9. I.F. Silvera and V.V. Goldman, *J. Chem. Phys*. **69**, 4209 (1978).
10. Yu.A. Freiman, A. Grechnev, S.M. Tretyak, A.F. Goncharov, and R.J. Hemley, *Phys. Rev. B* **86**, 014111 (2012).
11. E.S. Yakub, *Int. J. Thermophys*. **22**, 505 (2001).
12. E.S. Yakub, *Fiz. Nizk. Temp*. **26**, 350 (2000) [*Low Temp. Phys*. **26**, 240 (2000)].
13. E.S. Yakub, *J. Low Temp. Phys*. **122**, 559 (2001).

14. E.S. Yakub, *High Temp*. **28**, 664 (1990).
15. S. Zinn, D. Schiferl, and M.F. Nicol, *J. Chem. Phys*. **87**, 1267 (1987),
16. H.-J. Bohm and R. Ahlrichs, *J. Chem. Phys.* **77**, 2028 (1982).
17. W. Kolos and L. Wolniewitz, *J. Chem. Phys*. **41**, 3363 (1965); *ibid*. 43,2429 (1966).
18. W. Kolos and L. Wolniewitz, *J. Chem. Phys*. **49**, 404 (1968).
19. J.C. Slater, *Quantum Theory of Molecules and Solids. Vol. 1: Electronic Structure of Molecules*, McGraw-Hill, N-Y. (1974).
20. D. Saumon and G. Chabrier, *Phys. Rev. A* **44**, 5122 (1990).
21. Y. Akahama, M. Nishimura, H. Kawamura, N. Hirao, Y. Ohishi, and K. Takemura, *Phys. Rev. B* **82**, 060101 (2010).
22. E.S. Yakub, *High Temp.* **33**, 687 (1995).
23. M. Eremets, A.G. Gavriliuk, N.R. Serebryanaya, I.A. Trojan, D. Dzivenko, R. Boehler, H.K. Mao, and R.J. Hemley, *J. Chem. Phys*. **121**, 11296 (2004).
24. Jmol: an open-source Java viewer for chemical structures in 3D. *http://www.jmol.org/*
25. G. Rastelli and E. Cappelluti, *Phys. Rev. B* **84**, 184305 (2011).
26. E. Gregoryanz, A.F. Goncharov, K. Matsuishi, H-K. Mao, and R.J. Hemley. *Phys. Rev. Lett*. **90**, 175701 (2003).
27. L.N. Yakub, *Fiz. Nizk. Temp*. **39**, 552 (2013) [*Low Temp. Phys*. **39**, 427 (2013).
28. E.S. Yakub, *arXiv:1303.3960* (2013).
29. I.F. Silvera and S. Deemyad, *Fiz. Nizk. Temp*. **35**, 413 (2009) [*Low Temp. Phys*. **35**, 318 (2009)].
30. S.M. Davis, A.B. Belonoshko, B. Johansson, N.V. Skorodumova, and A.C.T. van Duin, *J. Chem. Phys.* **129**, 194508 (2008).
31. M.I. Eremets and I.A. Troyan, *Nature Mater*. **10**, 927 (2011).
32. E.S. Yakub, *Fiz. Nizk. Temp.* **39**, 541 (2013) [*Low Temp. Phys*. **39**, 417 (2013)].